

# **Development of a solenoid spectrometer for nuclear astrophysical studies of fusion reactions near stellar energies**

B. Bucher, A. Howard, J. J. Kolata, Y. J. Li, A. Roberts, X. D. Tang, M. Wiescher, X. Fang

November 2017



The INL is a U.S. Department of Energy National Laboratory  
operated by Battelle Energy Alliance

# **Development of a solenoid spectrometer for nuclear astrophysical studies of fusion reactions near stellar energies**

**B. Bucher, A. Howard, J. J. Kolata, Y. J. Li, A. Roberts, X. D. Tang, M. Wiescher, X. Fang**

**November 2017**

**Idaho National Laboratory  
Idaho Falls, Idaho 83415**

**<http://www.inl.gov>**

**Prepared for the  
U.S. Department of Energy  
Under DOE Idaho Operations Office  
Contract DE-AC07-05ID14517**

# Development of a solenoid spectrometer for nuclear astrophysical studies of fusion reactions near stellar energies

X. Fang<sup>a,b,\*</sup>, B. Bucher<sup>b,c</sup>, A. Howard<sup>b,\*\*</sup>, J. J. Kolata<sup>b</sup>, Y. J. Li<sup>d</sup>, A. Roberts<sup>b</sup>, X. D. Tang<sup>e</sup>, M. Wiescher<sup>b</sup>

<sup>a</sup>*Sino-French Institute of Nuclear Engineering and Technology, Sun Yat-Sen University, Zhuhai 519082, P. R. China*

<sup>b</sup>*Joint Institute for Nuclear Astrophysics, Department of Physics, University of Notre Dame, Notre Dame, Indiana 46556, USA*

<sup>c</sup>*Idaho National Laboratory, Idaho Falls, Idaho 83415, USA*

<sup>d</sup>*Department of Nuclear Physics, China Institute of Atomic Energy, Beijing 102413, P. R. China*

<sup>e</sup>*Institute of Modern Physics, Chinese Academy of Science, Lanzhou, Gansu 730000, P. R. China*

---

## Abstract

A solenoid spectrometer for nuclear astrophysics (SSNAP), has been developed to study heavy-ion fusion reactions of astrophysical importance near stellar energies range. Charged particles follow helical trajectories within the strong magnetic field of a superconducting solenoid. The  $^{12}\text{C}(^{12}\text{C},\text{p})^{23}\text{Na}$  reaction was studied as the first measurement of the solenoid spectrometer at the University of Notre Dame within the energy range of  $E_{\text{c.m.}}=4.0$  to 6.0 MeV. This experiment verified that the solenoid spectrometer is able to provide outstanding capacity for detection of light charged particles produced by nuclear fusion reactions having a relatively wide energy range.

*Keywords:* nucleosynthesis, solenoid spectrometer, magnetic field,

$^{12}\text{C}(^{12}\text{C},\text{p})^{23}\text{Na}$ , PSSD, SSNAP

---

\*fangx26@mail.sysu.edu.cn

\*\*Current address: Heinz Maier-Leibnitz Zentrum (MLZ), FRM-II, Technische Universität München, D-85748 Garching, Germany

## 1. Introduction

Fusion reactions involving  $^{12}\text{C}$  and  $^{16}\text{O}$  at low energies are of great astrophysical importance for understanding the nucleosynthesis during late stellar evolution[1]. The main challenge in experimental nuclear astrophysics is how to measure the extremely small cross sections with enough precision near Gamow peak energies. Examples of these reactions, such as  $^{12}\text{C}+^{12}\text{C}$ ,  $^{12}\text{C}+^{16}\text{O}$  and  $^{16}\text{O}+^{16}\text{O}$  that characterize the carbon burning and later oxygen burning phases of massive stars ( $M \geq 8M_{\odot}$ ), are crucial in a wide variety of stellar burning scenarios[1, 2]. Carbon burning in the core of stars occurs at temperatures of  $T=0.6-1.0$  GK, depending on the mass of the star, corresponding to center of mass energies between 1.0 and 3.5 MeV. The primary reaction channels and Q-values are  $^{12}\text{C}(^{12}\text{C},p)^{23}\text{Na}$  ( $Q = 2.24$  MeV),  $^{12}\text{C}(^{12}\text{C},\alpha)^{20}\text{Ne}$  ( $Q = 4.62$  MeV) and  $^{12}\text{C}(^{12}\text{C},n)^{23}\text{Mg}$  ( $Q = -2.60$  MeV) as shown in Fig.1. The stellar reaction rates determine the evolutionary paths of medium to massive stars and the associated nucleosynthesis. For massive stars the carbon burning rates affect the abundances of Ne, Na, Mg but impact also the production of heavier elements. It was shown that the production yields of  $^{26}\text{Al}$  and  $^{60}\text{Fe}$  in supernovae, two important galactic radioactive tracers, are sensitive to the carbon fusion rate[3]. The carbon fusion reaction is also considered to be responsible for igniting the explosions in type Ia supernovae[1]. Type Ia supernovae, as “standard candles”, are often used to measure precise distances of galaxies. In the late 1990s, distance measurements based on type Ia supernovae revealed that the universe expansion is accelerating[4, 5]. However, it has been discovered that Type Ia supernovae that were considered the same are in fact different. More precise study of formation mechanism of Type Ia supernovae leads to re-estimation of the expansion rate of the universe and the weight of dark energy.

Due to the exponentially decreasing cross section towards lower energies, precise experimental data of  $^{12}\text{C}+^{12}\text{C}$  fusion is difficult to be obtained at energies within the Gamow window. Therefore, the reaction rates rely on a number of extrapolations based on different model assumptions from reaction and struc-

ture theory. Not surprisingly, there are large discrepancies between the various model extrapolations. Traditionally, the optical model is used to fit the experimental data at higher energies and then predict the cross section values at the lower energies[2]. Recently, the hindrance model was proposed, introducing an additional term in the barrier potential[6]. This translates into a significant reduction of the cross sections towards lower energies. Moreover, strong narrow resonance structures were observed for the  $^{12}\text{C}+^{12}\text{C}$  cross sections at sub-barrier energies. The existence of such resonances in the Gamow window could substantially enhance the carbon burning reaction rate[7]. To remove these discrepancies and uncertainties in the theoretical predictions, measurements that can provide more precise data need to be extended to stellar energies.

The direct measurements of the emitted charged particles and  $\gamma$  rays are applied to provide reliable cross section values. For the direct measurement of  $^{12}\text{C}+^{12}\text{C}$ , due to the extremely small cross sections( $\sim\text{nb}$ ), particle- $\gamma$  ray coincidence methods are usually used to eliminate background. However, residual nuclei in their ground states can not be identified by coincidence methods because there are no  $\gamma$  rays emitted from them[8]. The importance of these nuclei is obvious, e.g. the weight of the  $^{23}\text{Na}$  ground state is about 30%-60% for the  $^{12}\text{C}(^{12}\text{C},\text{p})^{23}\text{Na}$  reaction at  $E_{cm}=1.0\text{-}3.0$  MeV. Therefore, a new method to collect light charged particles from fusion reactions at astrophysical energies has been proposed and proven to be efficient in this article. The solenoid spectrometer for nuclear astrophysics, uses the *TwinSol* solenoid system[9] at the University of Notre Dame to supply strong magnetic fields(up to 6 Tesla). This new experimental method can measure fusion reactions near stellar energies with relatively high efficiency through a simple detection setup. It is demonstrated that the strong magnetic field of such an instrument greatly reduces background from free electrons and multiple scattered beam particles. The  $^{12}\text{C}(^{12}\text{C},\text{p})^{23}\text{Na}$  reaction is the first measurement using the solenoid spectrometer.

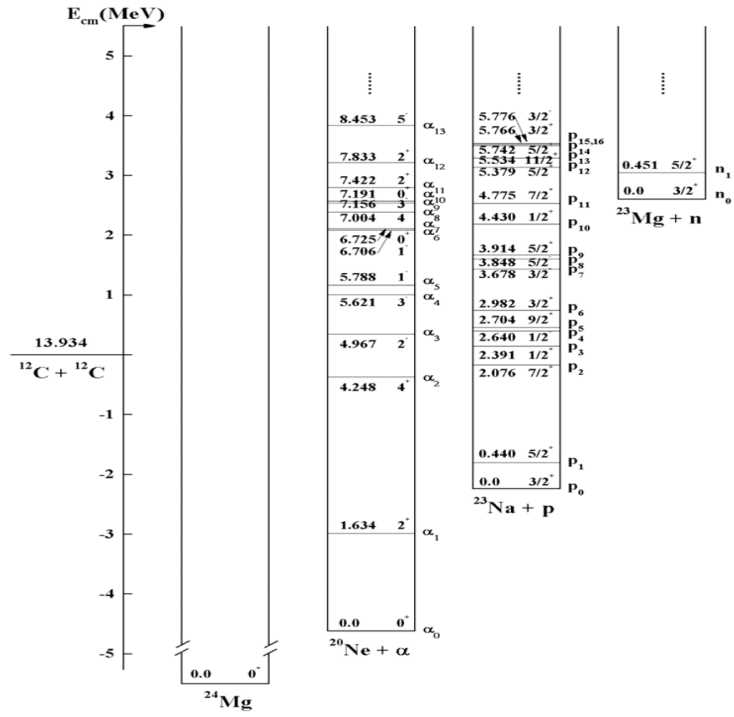


Figure 1: The primary reaction channels of  $^{12}\text{C} + ^{12}\text{C}$  fusion.  $p_i$  and  $\alpha_i$  represent the protons produced with  $^{23}\text{Na}$  and  $\alpha$  produced with  $^{20}\text{Ne}$  at the  $i$ th excited state  $i=0,1,2,3\dots$

## 59 2. Experimental Procedure

### 60 2.1. The concept

61 The solenoid spectrometer of the Nuclear Science Laboratory(NSL) at the  
62 University of Notre Dame was inspired by the first helical orbit spectrometer in  
63 the world, HELIOS at Argonne National Laboratory. The detailed concept is  
64 described in Ref.[10]. HELIOS was built and demonstrated powerful abilities of  
65 investigating reactions in inverse kinematics. We have been building a similar  
66 spectrometer using the existing *TwinSol* system at NSL[9]. The solenoid spec-  
67 trometer is based on the concept that charged particles undergo helical motion  
68 resulting from the Lorentz force in a uniform magnetic field. To realize this  
69 concept, the target and silicon detectors are both placed along the solenoid axis  
70 in the field. Thus, the charged particles emitted from the target move along  
71 helical orbits, and are then bent back and collected by position sensitive sili-  
72 con detectors oriented along the solenoid axis. All particles with relatively low  
73 momentum, so that their orbits do not exceed the solenoid chamber inner ra-  
74 dius, will consequently return to the axis. A schematic drawing of the proposed  
75 spectrometer is shown in Fig.2. It shows the recoil measurement setup that  
76 covers about  $2\pi$  solid angle, and can be easily converted to another setup by  
77 placing the silicon detectors after the target. The silicon detectors measure the  
78 particle's energy, distance from the target, and time of flight(TOF). With the  
79 energy and target-to-detector distance information, it is possible to reconstruct  
80 the emitted angles and the excitation energies of the coupled reaction residu-  
81 als. Compared to the traditional detection method, the solenoid spectrometer  
82 could provide much better energy resolution and a larger solid angle close to  
83  $4\pi$ , resulting in high-detection efficiency and excellent particle identification. A  
84 proof-of-principle measurement of the  $^{12}\text{C}+^{12}\text{C}$  fusion reaction was performed  
85 at energies  $E_{\text{c.m.}} = 4.0, 5.0$  and  $6.0$  MeV, providing spectra of proton and  $\alpha$   
86 particles from the  $^{12}\text{C}(^{12}\text{C},\text{p})^{23}\text{Na}$  and  $^{12}\text{C}(^{12}\text{C},\alpha)^{20}\text{Ne}$ .

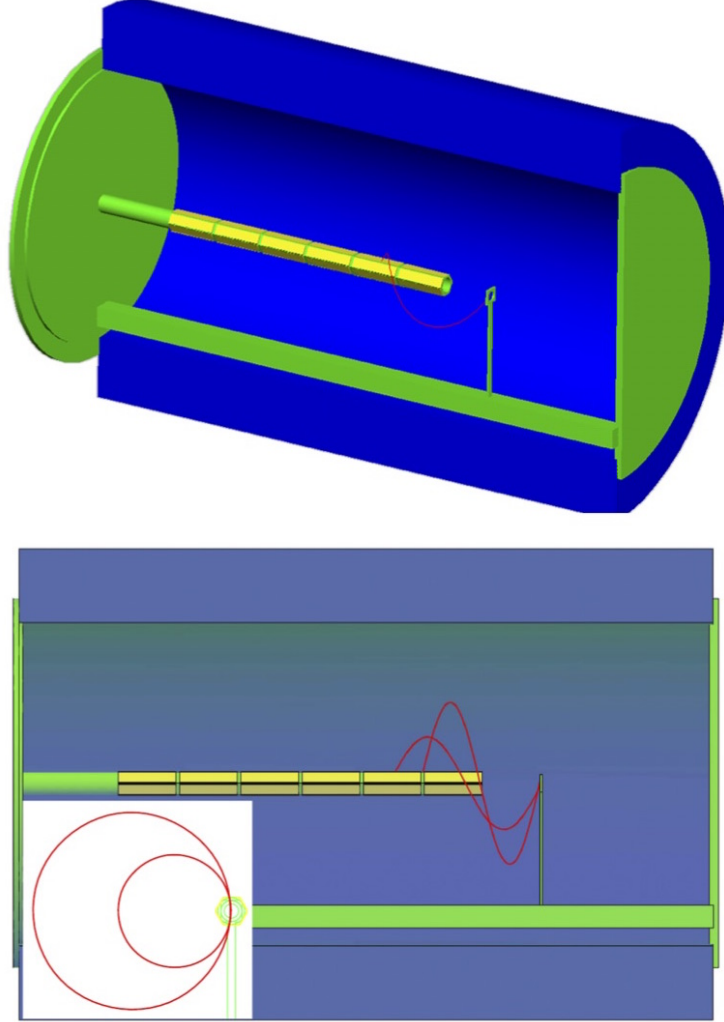


Figure 2: The schematic of the designed solenoid spectrometer. The beam particles travel from left to right through the hollow tube along the axis of the solenoid and hit the target, the position of which is adjustable along a track. The reaction products (red spiral) at backward angles are emitted and bent back to the axis after one cyclotron period; the left-bottom small figure shows the backside view. The position-sensitive silicon detector array (yellow segments), with a total length of 31 cm and a radius of 1.2 cm located around the axis, records energy, distance between target position and particle detected position, and the TOF with respect to beam pulses.

87 2.2. The setup for the first measurement with solenoid spectrometer

88 The core part of the solenoid spectrometer is the superconducting solenoid,  
 89 which is liquid-helium cooled, that provides magnetic fields. Each solenoid of  
 90 *TwinSol* includes a 30 cm bore with the capability of producing central fields  
 91 up to 6 Tesla in strength. The NbTi coil of each solenoid is 60 cm long with an  
 92 inner radius of 17.8 cm and an outer radius of 20.4 cm. To investigate the non-  
 93 uniformity of the field, the field map was calculated and shown in Fig. 3. The  
 94 radial symmetry is better than  $10^{-4}$ . The effects of field non-uniformities along  
 95 the solenoid field axis have been investigated through Monte Carlo simulations.  
 96 The results are shown in Fig. 6(bottom).

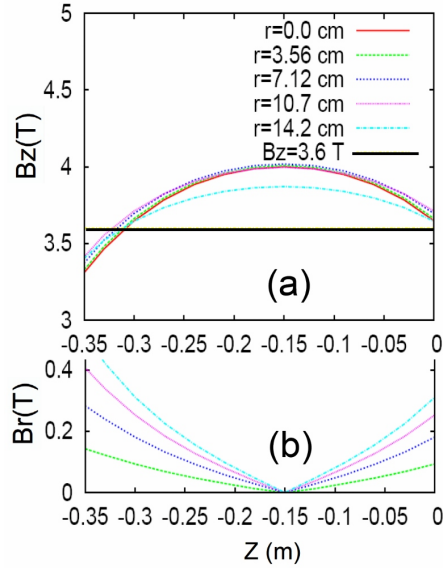


Figure 3: Map of the solenoid magnetic field components  $B_z$ ,  $B_r$ . Axial (a) and radial (b) are components of a *TwinSol* solenoid at several radial distances  $R$  from the solenoid axis. The central field is set to be 4.0 Tesla. The center of the field is shifted to the position of  $z = -0.15$  m. The target is located at the origin while the detector array covers the range from  $z = -0.05$  m to  $z = -0.35$  m. The horizontal line in the plot (a) corresponds to 90% of the central axial field value. Through the entire range, the radial component is less than 10% of the magnitude of the magnetic field.

97 Fig.4 presents the experimental setup of the solenoid spectrometer. A 20

98  $\mu\text{g}/\text{cm}^2$  thick graphite foil was placed at an adjustable location around the  
 99 center of the solenoid, as the target. Two one-dimensional position sensitive  
 100 silicon detectors(PSSD) were mounted onto the surface of a one-inch diameter  
 101 aluminum tube along the field axis in the upstream direction with respect to  
 102 the target. Each silicon detector was of  $5\text{ cm} \times 1\text{ cm}$  size. The distance between  
 103 the nearest edge of silicon detector and the target was arranged as 8 cm in the  
 104 test measurement. Two 5mm-diameter circular collimators were installed at  
 105 upstream and downstream positions respective to the target for improving the  
 106 beam-tuning. The detection setup was contained within the second solenoid.  
 107 Meanwhile, the focusing capability of the first solenoid was used for improving  
 108 the beam optics and minimizing the size of the beam-spot on target.

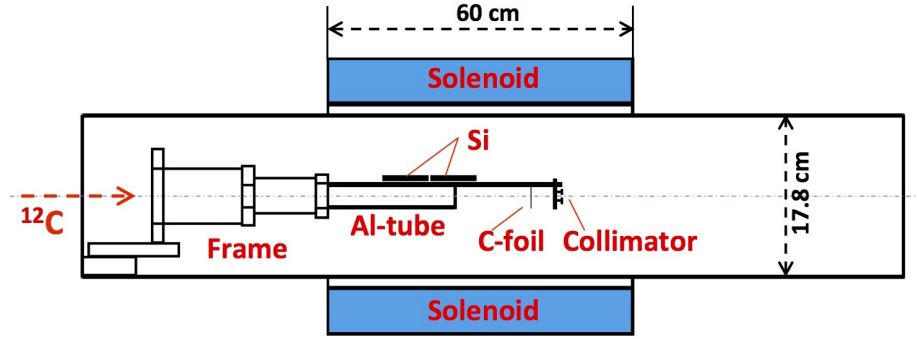


Figure 4: The schematic of the solenoid spectrometer setup for the first measurement of  $^{12}\text{C}(^{12}\text{C}, p)^{23}\text{Na}$ .

109 The energy signals from the silicon detector were processed by *Canberra*  
 110 203T pre-amplifiers followed by an *Ortec* 572 amplifier. The shaping time of the  
 111 amplifier was set to be  $3\text{ }\mu\text{s}$  to fully collect the charges from the particle-induced  
 112 ionization in the silicon detectors. The four position signals were fed into a 8-  
 113 channel *Mesytec* preamplifier followed by a 16-channel *Mesytec* amplifier. The  
 114 shaping time of the amplifier was set to be  $2\text{ }\mu\text{s}$ . Initially, the magnetic field  
 115 of the solenoid was brought up step-by-step by increasing the current, while  
 116 the performance of the solenoid spectrometer was evaluated using an  $^{241}\text{Am}$ -  
 117  $^{148}\text{Gd}$  mixed  $\alpha$ -source at the target position. The energy resolution was 54 keV

(FWHM) for 5.486 MeV  $\alpha$  particles. The position resolution was about 1 mm (FWHM). Then, the  $\alpha$  source was replaced by the target, and the  $^{12}\text{C}$  beam of  $\sim 3$  enA was added.

### 2.3. The $^{12}\text{C}(^{12}\text{C}, p)^{23}\text{Na}$ measurement

The performance of the solenoid spectrometer was tested using the  $^{12}\text{C}(^{12}\text{C}, p)^{23}\text{Na}$  and  $^{12}\text{C}(^{12}\text{C}, \alpha)^{20}\text{Ne}$  reactions in the energy range of  $E_{c.m.}=4.0$  MeV to 6.0 MeV using a  $^{12}\text{C}$  beam from the FN tandem accelerator at the University of Notre Dame. The primary reaction channels of the  $^{12}\text{C}+^{12}\text{C}$  fusion are shown in Fig. 1. The magnetic field was set to be 4.0 Tesla for all measurements. The first spectrum recorded by the solenoid spectrometer, measured at  $E_{c.m.}=6.0$  MeV, is shown in Fig. 5. By comparing the first solenoid spectrometer spectrum with the prediction, which are the dashed lines calculated using equation Eq. 1, we have identified several lines corresponding to the proton and  $\alpha$  particles produced with excited states of  $^{23}\text{Na}$  and  $^{20}\text{Ne}$ , e.g.  $\alpha_3$ ,  $\alpha_4$ ,  $\alpha_5$  and  $\alpha_6$ ,  $p_7$ ,  $p_{8,9}$ ,  $p_{10}$  and  $p_{11}$ . Besides those proton and  $\alpha$  lines, there are several low-energy wide bands with intensities that are much stronger than the proton and  $\alpha$  particles. These background signals are suspected to be multiple-scattered  $^{12}\text{C}$  from the upstream setup. Thus, the quality of the measurement required improvements.

To remove the background content and avoid the intersection between the proton and  $\alpha$  particle lines, Mylar and aluminum foils were placed in front of the PSSDs to absorb the scattered  $^{12}\text{C}$  beam particles and  $\alpha$  particles from  $^{12}\text{C}(^{12}\text{C}, \alpha)^{20}\text{Ne}$ . This helped to achieve clean spectra for measurement at beam energies  $E_{c.m.}=4.0$ , 5.0 and 6.0 MeV. The E-(-z) spectrum measured at  $E_{c.m.}=5.0$  MeV is shown in Fig. 6(top). It shows the combination of measurements with two different target locations. The detector array covers a distance of 10 cm. To cover a longer range, the measurement was done by placing the target at two different locations. The covered distance from the target is between -0.08 m and -0.18 m for the first location and between -0.24 m and -0.34 m for the second location. A 5.4- $\mu\text{m}$  thick Mylar degrader was used at the first location. It was replaced by a 5.7- $\mu\text{m}$  Aluminum foil at the second location. Because of the

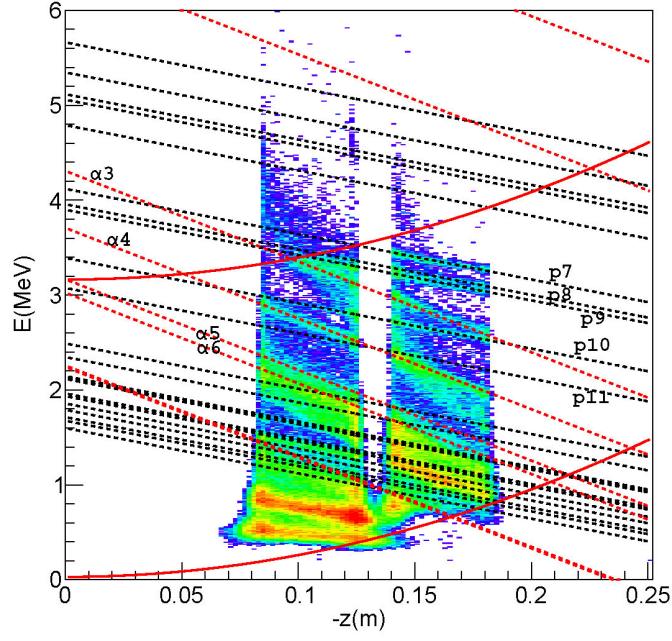


Figure 5: The energy ( $E$ ) vs. position ( $-z$ ) spectrum measured at  $E_{c.m.}=6.0$  MeV. The target horizontal position along the solenoid axis was defined as  $z=0$ , and the position  $z$  of products is positive (negative) if they were emitted after (before) the target. In this work all particles were measured at backward angles, thus the x-axis title name is ' $-z$ '. The predicted lines corresponding to the excited states in  $^{23}\text{Na}$  and  $^{20}\text{Ne}$  are shown in black and red dashed lines, respectively. To match the observation, the magnetic field used in the prediction was set as 4.4 Tesla, 10% higher than the actual field, to compensate the effect incurred by the half inch distance of the detectors with respect to the solenoid center. The region between the two solid red lines shows the capacity to detect protons for a given magnetic field and fixed solenoid chamber radius[10].

energy loss in the degrader, the correlation between energy (E) and position (-z) deviates from the predicted straight lines, especially at larger distance from the detectors.

#### 2.4. The simulation

The simulation of the detector performance is an important aspect for experiments. To address the influence of the strong magnetic field, the sensitivity to detector position and field inhomogeneities, a Monte Carlo simulation code using *GEANT4* was developed for the present work. First, a constant 4 Tesla magnetic field is used in the simulation. The predicted lines for various excited states are calculated using the following equation,

$$E_a = \left( \frac{E_{beam}}{2} + Q_0 - E_x \right) \times \frac{24 - a}{24} - \frac{1}{2} m_a V_{cm}^2 + \left( \frac{m_a V_{cm}}{T_{cyc}} \right) z \quad (1)$$

where  $E_{beam}$  is the incident  $^{12}\text{C}$  beam energy;  $Q_0$  is the reaction Q-value for the channel decaying to the ground states and is equal to 2.24 MeV for  $^{12}\text{C}(^{12}\text{C}, p)^{23}\text{Na}$  and 4.617 MeV for  $^{12}\text{C}(^{12}\text{C}, \alpha)^{20}\text{Ne}$ , respectively;  $E_x$  is the excitation energy for the fusion residuals, e.g.  $^{23}\text{Na}$ ,  $^{20}\text{Ne}$ ;  $m_a$  is the mass number in *amu* for the detected light particle (1 for proton, and 4 for  $\alpha$ );  $V_{cm}$  is the speed in the center of mass reference frame;  $z$  is the position at which the light particle is detected by the detectors, where  $z=0$  is the target position;  $T_{cyc}$  is the cyclotron period for the detected light particle which can be calculated using the following equation,

$$T_{cyc} = 65.6 \times \frac{a}{Bq} \text{ (ns)} \quad (2)$$

where  $a$  is the mass number in *amu*,  $B$  is the magnetic field in Tesla and  $q$  is the ion charge in unit of  $e$ . It was found that the detected protons and  $\alpha$  particles took shorter flight times than the calculated  $T_{cyc}$ , due to the added distance between detectors and the solenoid axis (see Fig. 2). To match the simulation,

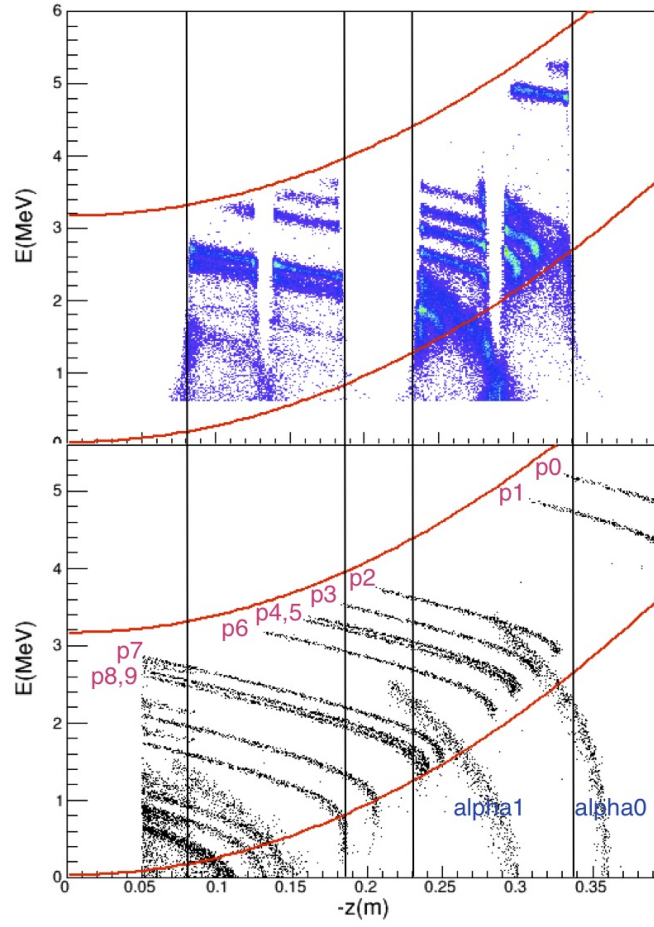


Figure 6: (top) The energy ( $E$ ) vs. position ( $-z$ ) spectrum measured at  $E_{cm}=5.0$  MeV. (bottom) Simulation using *GEANT4*. The region between the two solid red lines highlights the detection range for protons and  $\alpha$  particles produced from  $^{12}\text{C}+^{12}\text{C}$  based on the experimental magnetic field and solenoid chamber radius.

the magnetic field used in the prediction are increased by 10% to compensate for the shorter flight times.

The simulated energy (E) vs. position (-z) spectrum using *GEANT4* is shown in Fig. 6(bottom). The coverage of detector is marked by two red lines. The  $\alpha$  lines, shown in black wide bands, correspond to the  $\alpha_0$ ,  $\alpha_1$  and  $\alpha_2$ . The proton lines, shown in black narrow bands, correspond to  $p_0$ ,  $p_1$ ,  $p_2$ ,  $p_3$ ,  $p_{4,5}$ ,  $p_6$ ,  $p_7$ ,  $p_{8,9}$ ,  $p_{10}$  and  $p_{11,12}$ . The proton lines under  $\alpha_2$  are not observed in the experiment due to their low energies. Comparing with the results in Fig. 6(top), the simulation matches very well with the present measurement.

### 3. Results and discussion

#### 3.1. Analysis of data without any detector shield

The present experimental data provides energy(E) and position(z) information of light charged particles (p,  $\alpha$ ). The Q-values for different excited states in  $^{23}\text{Na}$  and  $^{20}\text{Ne}$  are reconstructed by solving the equation Eq. 1. The corresponding spectra of Q-values are shown in Fig. 7. With the measured energies(e) and positions(z) for the protons and  $\alpha$  particles, it is possible to determine the excited energy for the residuals, *i.e.*  $^{23}\text{Na}$  and  $^{20}\text{Ne}$ . The excitation energy spectrum for the  $p+^{23}\text{Na}$  channel is shown in Fig. 7(a)(c). The excitation energy spectrum for the  $\alpha+^{20}\text{Ne}$  channel is shown in Fig.7(b)(d). The energy resolution for the peak corresponding to the  $E_x=3.97$  MeV state in  $^{23}\text{Na}$  is determined as 65 keV (FWHM). The doublets ( $p_8$  and  $p_9$ ) in Fig.7(c),  $E_x=3.85$  MeV and 3.91 MeV, are clearly separated. However, the resolution for the  $\alpha$  peaks, which correspond to the  $E_x=4.24$  MeV and  $E_x=4.97$  MeV states in  $^{20}\text{Ne}$ , are 120 keV; much worse than the resolution of the protons. With the detected  $\alpha$  particle energy varying between 2.0 and 4.0 MeV, this poor resolution may result from the energy loss of  $\alpha$  particles in the target and the dead layer of the silicon detectors.

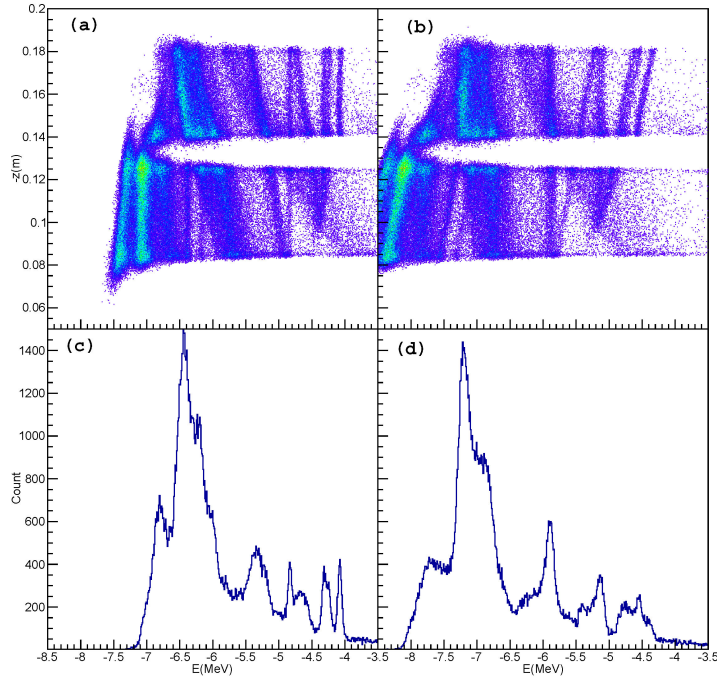


Figure 7: The reconstructed excitation energy spectra for the  $p+^{23}\text{Na}$  and the  $\alpha+^{20}\text{Ne}$  channels at  $E_{c.m.}=6.0$  MeV. (a) The position( $-z$ ) vs.  $Q$ -values( $E$ ) of the  $p+^{23}\text{Na}$ . (b) The position( $-z$ ) vs.  $Q$ -values( $E$ ) of the  $\alpha+^{20}\text{Ne}$ . (c) is the projection of the spectrum in (a); (d) is the projection of the spectrum in (b).

### 198 3.2. Analysis of data with detector shield

199 To achieve clean proton spectra, a detector shield was applied to eliminate  
 200 the scattered  $^{12}\text{C}$  beam and  $\alpha$  particles. Nevertheless, protons would lose ener-  
 201 gies when going through the shield foil. To correct the energy loss in the foil,  
 202 the angle  $\theta_{lab}$  is reconstructed from the detected energy (E) and position (z)  
 203 information using the equation,

$$\cos(\theta_{lab}) = \frac{z}{T_{cyc}} \sqrt{\frac{m}{2E}} \quad (3)$$

204 where  $T_{cyc}$  is the cyclotron period for protons,  $\theta_{lab}$  is the emitted angle of pro-  
 205 tons with respect to the beam incident direction. With the  $\theta_{lab}$  values, the  
 206 corresponding effective thickness of foil is obtained from the actual thickness  
 207 divided by the angle correction factor,  $\sin(\theta_{lab})$ . Then the proton energy could  
 208 be corrected by summing the detected energy with the energy loss in the foil.  
 209 The energy(E) vs. angle( $\theta_{cm}$ ) of protons at  $E_{cm}=5.0$  MeV is shown in Fig. 8.  
 210 It is still a combination of two measurements with different target locations.  
 211 A broad angle coverage from  $120^\circ$  to  $170^\circ$  is observed with the present simple  
 212 setup. Fig. 9 shows the angular distributions of separated proton groups, which  
 213 are labeled. The red curves are the angular distribution fit results from a previ-  
 214 ous measurement, which was carried out using a large area strip silicon detector  
 215 array[8].

216 The position(-z) vs. Q-values( $E_{qval}$ ) spectrum measured at  $E_{cm}=5.0$  MeV is  
 217 shown in Fig.10(top). A cut is applied to the -z vs.  $E_{qval}$  spectrum in Fig.10 to  
 218 select a subset of events to generate the clear projection of proton peaks. The  
 219 identified peaks are labeled.

## 220 4. Conclusion

221 This work demonstrated that the solenoid spectrometer is able to provide  
 222 outstanding capacity to study nuclear fusion reactions for a relatively wide en-  
 223 ergy range through the measurement of charge-particle channels from  $^{12}\text{C}+^{12}\text{C}$   
 224 fusion, especially the  $^{12}\text{C}(^{12}\text{C}, p)^{23}\text{Na}$  reaction. Both good energy resolution

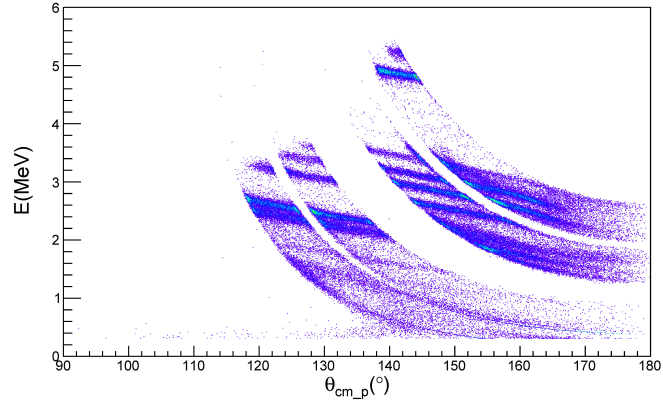


Figure 8: The energy ( $E$ ) vs. angle( $\theta_{cm}$ ) spectrum measured at  $E_{cm}=5.0$  MeV.

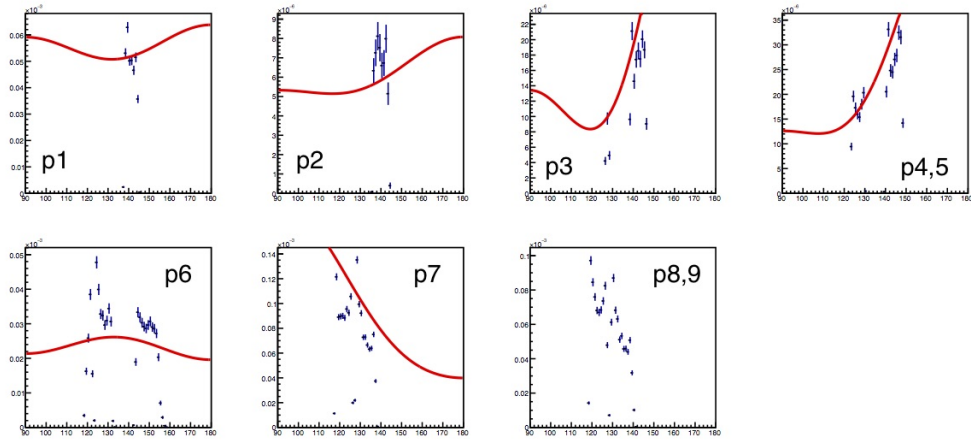


Figure 9: The angular distribution ( $d\sigma/d\Omega$  vs.  $\theta_{cm}$ ) spectrum of different proton peaks measured at  $E_{cm}=5.0$  MeV.

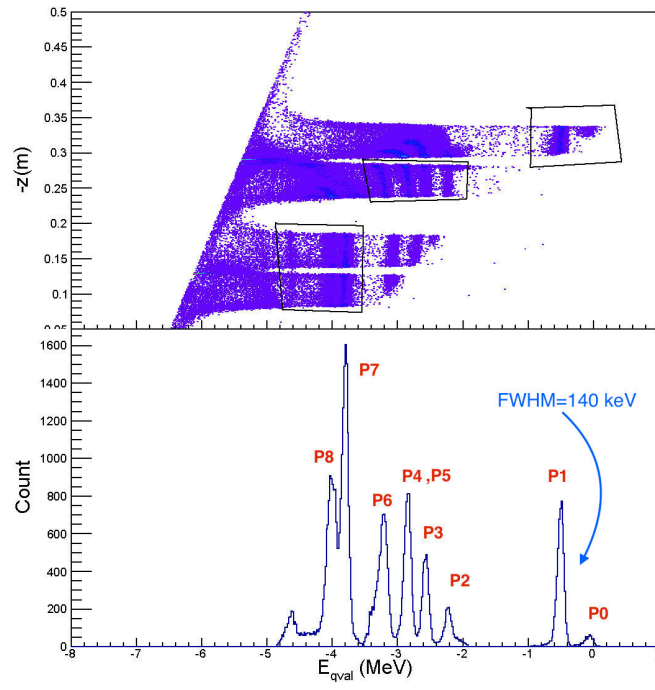


Figure 10: The position( $-z$ ) vs.  $Q$ -values( $E_{qval}$ ) spectrum measured at  $E_{cm}=5.0$  MeV (top). Three regions (in black boxes) including some identified proton lines are chosen to provide the projection (bottom). The FWHM of  $p_1$  peak is about 140 keV.

and angular resolution were achieved from the simple setup described. The solenoid spectrometer can be applied to a broad variety of sub-Coulomb barrier nuclear reactions with substantially larger efficiency than traditional detection methods. This project is being pursued further by the development of an extended silicon detection array along the solenoid axis. Upgrades were recently applied to *TwinSol*, including a multi-cell gas target and a possible third solenoid, and the final design of SSNAP is being determined[11].

## 5. Acknowledgments

This work was supported by the National Science Foundation under Grant Nos. PHY-1419765 and PHY14-01343, the Joint Institute of Nuclear Astrophysics Center for the Evolution of the Elements grant under Grant No. PHY-1430152, the National Natural Science Foundation of China under Grant Nos. 11321064 and 11205247 and the Fundamental Research Funds for the Central Universities under Grant No. 17lgzd34.

## References

- [1] C. E. Rolfs, W. S. Rodney, *Cauldrons in the cosmos: Nuclear astrophysics*, University of Chicago press, 1988.
- [2] C. Iliadis, *Nuclear physics of stars*, John Wiley & Sons, 2015.
- [3] M. Limongi, A. Chieffi, *Nuclear Physics A* 758 (2005) 11–14.
- [4] A. G. Riess, A. V. Filippenko, P. Challis, A. Clocchiatti, A. Diercks, P. M. Garnavich, R. L. Gilliland, C. J. Hogan, S. Jha, R. P. Kirshner, et al., *The Astronomical Journal* 116 (3) (1998) 1009.
- [5] S. Perlmutter, G. Aldering, G. Goldhaber, R. Knop, P. Nugent, P. Castro, S. Deustua, S. Fabbro, A. Goobar, D. Groom, et al., *The Astrophysical Journal* 517 (2) (1999) 565.

- 250 [6] C. L. Jiang, K. E. Rehm, B. B. Back, R. V. F. Janssens, Phys. Rev. C 75  
251 (2007) 015803.
- 252 [7] R. L. Cooper, A. W. Steiner, E. F. Brown, Astrophysical J. 702 (2009)  
253 660–671.
- 254 [8] X. Fang, B. Bucher, S. Almaraz-Calderon, A. Alongi, A. Ayangeakaa,  
255 A. Best, G. Berg, C. Cahillane, E. Dahlstrom, M. Freer, et al., in: Journal  
256 of Physics: Conference Series, Vol. 420, IOP Publishing, 2013, p. 012151.
- 257 [9] J. Kolata, A. Morsad, X. Kong, R. Warner, Nucl. Instr. and Meth. B 40-41  
258 (1989) 503–506.
- 259 [10] A. Wuosmaa, J. Schiffer, B. Back, C. Lister, K. Rehm, Nucl. Instr. and  
260 Meth. A 580 (2007) 1290–1300.
- 261 [11] P. O’Malley, D.W.Bardayan, J. Kolata, M. Hall, O. Hall, J. Allen, F. Bec-  
262 chetti, the TwinSol collaboration, Nucl. Instr. and Meth. B 376 (2016)  
263 417–419.